Astronomy & Astrophysics manuscript no. ms˙arxiv
November 1, 2010

Timing of the accreting millisecond pulsar IGR J17511–3057

A. Riggio[1,2], A. Papitto[1,2], L. Burderi[2], T. Di Salvo[3], M. Bachetti[2], R. Iaria[3], A. D'Aì[3], and M.T. Menna[4]

[1] INAF/Osservatorio Astronomico di Cagliari, località Poggio dei Pini, strada 54, 09012 Capoterra, Italy; e-mail: ariggio@oa-cagliari.inaf.it
[2] Università di Cagliari, Dipartimento di Fisica, SP Monserrato-Sestu km 0,7, 09042 Monserrato (CA), Italy
[3] Dipartimento di Scienze Fisiche e Astronomiche, Università di Palermo, Via Archirafi 36, Palermo, 90123 Italy
[4] Osservatorio Astronomico di Roma, Sede di Monteporzio Catone, Via Frascati 33, Roma, 00040 Italy

Abstract

Context. Timing analysis of Accretion-powered Millisecond Pulsars (AMPs) is a powerful tool to probe the physics of compact objects. The recently discovered IGR J17511–3057 is the 12 discovered out of the 13 AMPs known. The Rossi XTE satellite provided an extensive coverage of the 25 days-long observation of the source outburst.

Aims. Our goal is to investigate the complex interaction between the neutron star magnetic field and the accretion disk, determining the angular momentum exchange between them. The presence of a millisecond coherent flux modulation allows us to investigate such interaction from the study of pulse arrival times. In order to separate the neutron star proper spin frequency variations from other effects, a precise set of orbital ephemeris is mandatory.

Methods. Using timing techniques, we analysed the pulse phase delays fitting differential corrections to the orbital parameters. To remove the effects of pulse phase fluctuations we applied the timing technique already successfully applied to the case of an another AMP, XTE J1807–294.

Results. We report a precise set of orbital ephemeris. We demonstrate that the companion star is a main sequence star. We find pulse phase delays fluctuations on the first harmonic with a characteristic amplitude of about 0.05, similar to what also observed in the case of the AMP XTE J1814–338. For the second time an AMP shows a third harmonic detected during the entire outburst. The first harmonic phase delays show a puzzling behaviour, while the second harmonic phase delays show a clear spin-up. Also the third harmonic shows a spin-up, although not highly significant (3σ c.l.). The presence of a fourth harmonic is also reported. In the hypothesis that the second harmonic is a good tracer of the spin frequency of the neutron star, we find a mean spin frequency derivative for this source of $1.65(18) \times 10^{-13}$ Hz s^{-1}.

Conclusions. In order to interpret the pulse phase delays of the four harmonics, we applied the disk threading model, but we obtained different and not compatible $\dot{M}$ estimates for each harmonic. In particular, the phase delays of the first harmonic are heavily affected by phase noise, and consequently, from these data, it is not possible to derive a reliable estimate of $\dot{M}$. The second harmonic gives a $\dot{M}$ consistent with the flux assuming that the source is at a distance of 6.3 kpc. The third harmonic gives a lower $\dot{M}$ value, with respect to the first and second harmonic, and this would reduce the distance estimate to 3.6 kpc.

Key words. stars: neutron – stars: magnetic fields – pulsars: general – pulsars: individual: IGR J17511–3057 – X-ray: binaries.

1. Introduction

Accretion-powered millisecond pulsars (hereafter AMPs) are transient low mass X-ray binaries, which show a coherent modulation of their X-ray fluxes with periods of the order of few milliseconds. In the recycling scenario AMPs are seen as the progenitors of the millisecond radio pulsars (see e.g. van den Heuvel 1984), the accretion process being responsible for the spinning up of the neutron star (hereafter NS) to milliseconds periods.

The AMP IGR J17511–3057 was discovered by *INTEGRAL* on 12 September, 2009 during a galactic bulge monitoring (Baldovin 2009). Although very close to the previously known AMP XTE J1751–305, the source position measured by *INTEGRAL* suggested it was a newly discovered X-ray source. The observation of a coherent modulation of the X-ray flux in the data from a ToO observation performed by the Rossi X-ray Timing Explorer (hereafter *RXTE*) with a period of about 4 ms (Markwardt et al. 2009b) permitted to classify IGR J17511–3057 as an AMP and confirmed it as a new transient X-ray source. Altamirano et al. (2010) reported the presence of burst oscillations at the NS frequency. An analysis of a Chandra observation by Nowak et al. (2009) gave the best source position with an uncertainty of 0.6″. IGR J17511–3057 was observed by *Swift* (Bozzo et al. 2009), producing a description of the X-ray spectrum. Torres et al. (2009) reported a possible near-infrared counterpart. A detailed spectral analysis and a set of orbital parameters were given by Papitto et al. (2010) analysing a ToO *XMM–Newton* observation. Riggio et al. (2009), analysing a *RXTE* observation, refined the orbital parameters. Very recently Miller-Jones et al. (2009) set an upper limit on the radio emission. Surprisingly, another transient X-ray source (XTE J1751–305) went into outburst very near the position of IGR J17511–3057 on 7 October, 2009 (Chenevez et al. 2009) and its pulsations was detected by *RXTE* (Markwardt et al. 2009a) while observing IGR J17511–3057. IGR J17511–3057 has faded under detection threshold on 8 October, 2009.

In this work we present a detailed timing analysis of the *RXTE* ToO observation of the source IGR J17511–3057.

2. Observation and Data Analysis

In this work we analyse *RXTE* observation of IGR J17511–3057. In particular, we use data from the PCA (proportional counter array) instrument on board of the *RXTE* satellite (ObsId P94041

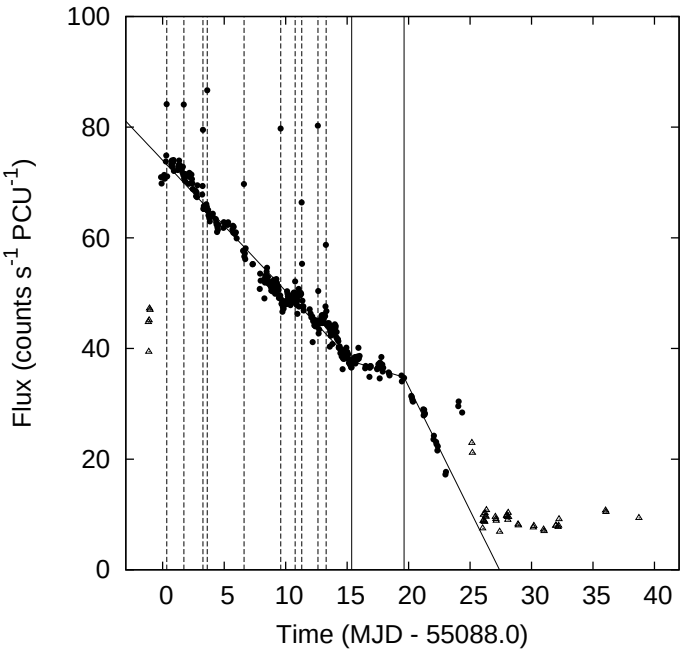

Figure 1. PCU 2 count rate (2–25 keV), subtracted of the background, is reported as a function of time during the outburst. The superimposed model represents the best fit using a piecewise linear function. The abrupt flux raise at the end of the outburst is due to the onset of an outburst from the AMP XTE J1751–305. The dashed vertical lines are in correspondence of the type-I bursts present in the observation while the continuous vertical lines are in correspondence of the slope change accordingly to the model used to describe the count rate. The filled circles are relative to the ObsId 94041, while the triangles are the XTE J1751–305 observation (ObsId 94042)

and P94042). We used data collected in event packing mode, with time and energy resolution of $122\mu s$ and 64 energy channels respectively. We selected data in the energy range 2-25 keV in order to maximise the signal to noise ratio, since above $\sim$ 20 keV the background dominates. The X-ray flux follows a piecewise linear decay as showed in Figure 1, with a peak flux of 70 counts s^{-1} PCU^{-1}. The re-brightening visible in Figure 1, 24 days after the start of the observation, is due to the AMP XTE J1751–305 in the field of view of *RXTE* going into outburst. The analysed data cover the time span from 12 September 2009 (MJD 55086.8) to 22 October 2009 (MJD 55126.8). We corrected the photon arrival times for the motion of the Earth-spacecraft system with respect to the Solar System barycentre and reported them to barycentric dynamical times at the Solar System barycentre using the *faxbary* tool (DE-405 solar system ephemeris). We used the *Chandra* source position reported by Nowak et al. (2009), and reported in Table 1. The uncertainty on the source position quoted by Nowak et al. (2009) is 0.6″, 1σ confidence level.

2.1. Derivation of the orbital ephemeris

To obtain a first estimate of the mean spin frequency we constructed a Fourier power density spectra of the first data file of the ObsID 94041-01-01-00 with a bin size of 2^{-11} seconds and on data segments of 64 seconds and averaging 53 power spectra. We found a strong signal at $\sim$ 244.81 Hz, in good agreement with the value reported by Markwardt et al. (2009b). We divided the observation in time intervals of about 400 seconds each and performed an epoch folding search on each data interval around

Table 1. Orbital and Spin Parameters for IGR J17511–3057.

Parameter	Value
RA (J2000), (Nowak et al. 2009)	$17^h\,51^m\,08\overset{s}{.}66$
Dec (J2000), (Nowak et al. 2009)	$-30^\circ\,57'\,41\overset{''}{.}0$
Orbital period, P_{orb} (s)	12487.5121(4)
Projected semi-major axis, $a_x \sin i$ (lt-ms)	275.1952(18)
Ascending node passage, T* (MJD)	55088.0320279(4)
Eccentricity, e	$< 3 \times 10^{-5}$
Mass function[(1)], f_x ($M_\odot$)	$1.070854(21) \times 10^{-3}$
Reference epoch, T_0 (MJD)	55088.0
Mean spin frequency, ν_0 (Hz)	244.83395156(7)
Constant $\dot\nu$ Model best fit parameters	
$\chi^2_r(\chi^2/\text{d.o.f.})$	1.74(238.5/137)
Spin frequency at T_0, ν_0 (Hz)	244.83395145(9)
Spin frequency derivative, $\dot\nu$ (Hz s^{-1})	$1.45(16) \times 10^{-13}$
Physical Model best fit parameters	
$\chi^2_r(\chi^2/\text{d.o.f.})$	1.70(232.8/137)
Spin frequency, ν_0 (Hz)	244.83395145(9)
Accretion rate at T_0 ($M_\odot$ year^{-1})	$0.92(10) \times 10^{-9}$

Errors are intended to be at 1σ c.l., upper limits are given at 95% confidence level. Times are referred to the barycentre of the Solar System (TDB). Best fit spin parameters are derived in both hypothesis of a constant spin-up and flux dependent spin-up, and the uncertainties on the given values of ν, $\dot\nu$ and $\dot{M}_{\rm max}$ include systematics due to the uncertainties in the source position (see text). Here we report only the second harmonic best fit spin parameters.
(1) This value was obtained using the latest available measure of G, c (`http://physics.nist.gov/cuu/Constants/`) and $M_\odot$ (`http://nssdc.gsfc.nasa.gov/planetary/factsheet/sunfact.html`).

the averaged spin period with a period resolution of 4×10^{-9} s. For each time interval we obtained an estimate of the best spin period. We excluded all the intervals for which the maximum in the χ^2 curve was not significant (3σ c.l.), according to the criterion stated by Leahy et al. (1983). A sinusoidal Doppler modulation of the spin period due to the source motion in the binary system was evident. We fitted the Doppler frequency shifts with the formula:

$$\nu(t) = \nu_0 + \dot\nu(t - T_0) - \frac{2\pi\,\nu_0\,A}{P_{\rm orb}} \cos l(t), \qquad (1)$$

where ν_0 is the spin frequency at the time T_0, $\dot\nu$ is the spin frequency derivative, A is the orbit projected semi-major axis over the speed of light and $l(t) = 2\pi(t - T_\star)/P_{\rm orb}$, where $T_\star$ is the time of passage through the ascending node and $P_{\rm orb}$ is the orbital period. With a reduced χ^2 (hereafter χ^2_r and defined as χ^2 / d.o.f.) of 0.59(532.2/898) we obtained a first set of orbital parameters and a much better estimate of the barycentric spin frequency.

Using this preliminary orbital solution we analyse the pulse phase delays to get a more precise estimate of the orbital and spin parameters. We epoch folded data on time intervals of about 1500 s using 32 phase channels. An example of the folded pulse profile is reported in Figure 2. An harmonic decomposition of each pulse profile up to the fourth harmonic was necessary. To do that we fitted each normalised pulse profile using the following expression:

$$f(\phi) = 1 + \sum_{n=1}^{4} a_n \sin(2n\pi(\phi - \phi_n)), \qquad (2)$$

where a_1, a_2, a_3 and a_4 are the sinusoidal semi-amplitudes (hereafter fractional amplitudes) of the first, second, third and fourth harmonics respectively and ϕ_1, ϕ_2, ϕ_3 and ϕ_4 the corresponding

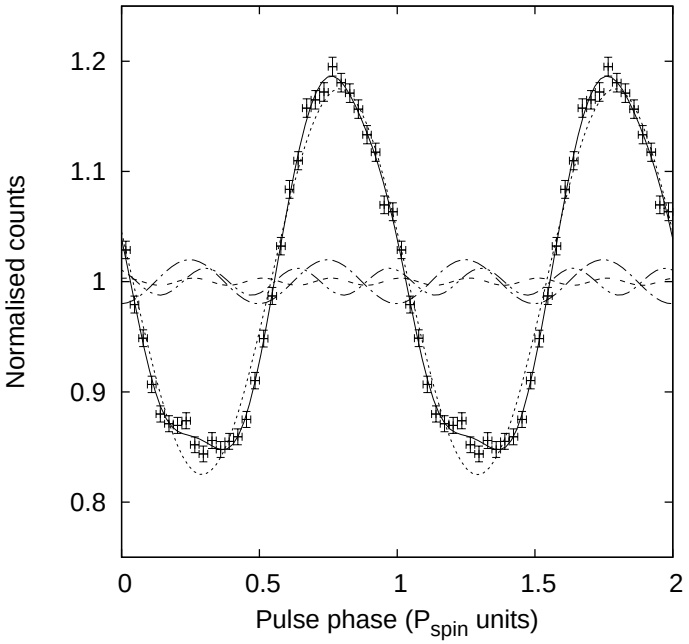

Figure 2. In this figure a folded pulse profile is reported. For clarity two spin cycles are plotted. The continuous line is the best-fit using first, second and third harmonics. We also reported the single contribution to the profile of the first harmonic (dotted line), second harmonic (dot-dashed line), third harmonic (bi-dot dashed line) and fourth harmonic (dashed line).

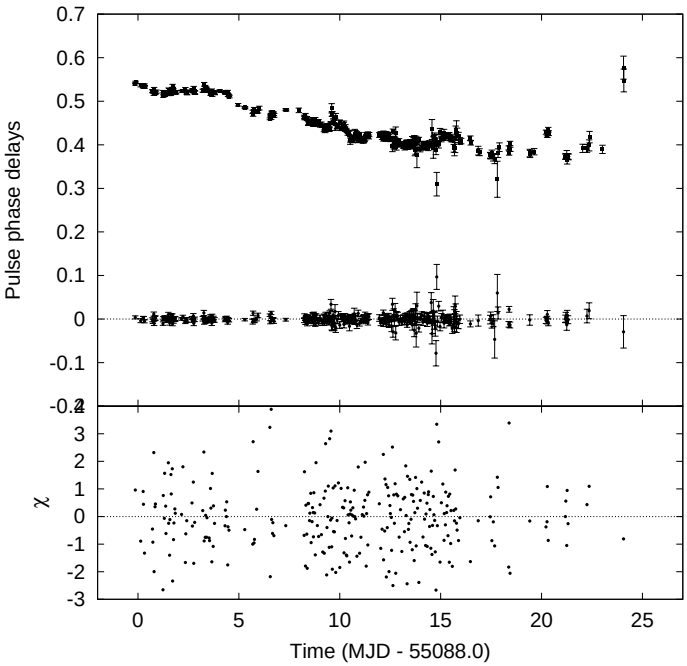

Figure 3. In the top panel of this figure the pulse phase delays (filled squares) and the corresponding pulse phase delay differences (filled circles) on the data corrected with the orbital ephemeris obtained from the fit of the frequency Doppler shifts are reported. Each pulse phase point is obtained by fitting the folded pulse profile over about 1500 s of data. It is evident that there is no trace of such fluctuation in the pulse phase delay differences, giving a striking confirmation of the goodness of the method. In the bottom panel are reported the residuals (in σ units) with respect to the best fit orbital solution derived from the pulse phase delay differences using the timing technique described in the text.

phases. We rejected the pulse phase delays for which the following two conditions were not both satisfied: i) the signal is not detected at least at a 3σ confidence level (Leahy et al. 1983); ii) the best fit fractional amplitude had to be at least at 3σ from zero ($a_i/\delta a_i \geq 3$).

We first tried to fit the pulse phase delays with a polynomial to describe the pulse phase delays long term fluctuations plus the usual formula $\phi_{orb}(t)$, describing the pulse phase residuals due to differential corrections to the initial orbital parameter estimates(Deeter et al. 1981, see e.g. Riggio et al. 2007).

We tried to describe the phase fluctuations using a polynomial up to the 9$^{\rm th}$ degree to fit obtaining a $\chi^2_r = 6.11(1834.6/300)$, which is formally unacceptable.

Due to the presence of these phase fluctuations we decided to apply the timing technique described in Riggio et al. (2007) in order to separate the orbital modulation from the phase fluctuations, to obtain a better estimates for the orbital parameters.

Following Riggio et al. (2007) we define the pulse phase differences as:

$$\Delta\phi_{orb}(t_i) = \phi_{orb}(t_{i+1}) - \phi_{orb}(t_i), \quad (3)$$

We excluded all the points for which $t_{i+1} - t_i > P_{\rm orb}$ in order to optimise the filter efficiency (Riggio et al. 2007).

We iterated the process until convergence. In the last iteration (see Figure 3) the $\chi^2_r = 1.43(398/279)$, which is much more better than the previous approach. The orbital ephemeris best-fit results are reported in Table 1, where the errors have been multiplied by the factor $\sqrt{\chi^2_r}$ (Bevington & Robinson 2003).

The values obtained are in perfect agreement with the ones reported by Papitto et al. (2009) from an analysis of a *XMM–Newton* observation and by Riggio et al. (2009), obtained with *RXTE* data but on a shorter time interval. The obtained uncertainties on the orbital parameters are a factor two smaller than the best orbital solution previously given by Riggio et al. (2009). Note also that the orbital period we derive here has a relative uncertainty as small as 0.03%.

In order to fit the pulse phase delays with a physically meaningful torque which takes into account the decreasing X-ray flux (and hence $\dot{M}$, in the hypothesis that the X-ray flux is a good tracer of the mass accretion rate onto the NS), we need to describe the flux evolution during the outburst, i.e. the bolometric flux at the peak of the outburst and the shape of the light curve.

In order to estimate the bolometric flux of the source at the peak of the outburst, we considered the spectrum collected by the PCA in Standard 2 Mode (129 energy channels recorded at a time resolution of 16s) during Obs. 94041-01-01-04, which started on 55089.283 MJD and had a total exposure of 10480s. We considered only data taken by the PCU2 in order to avoid cross-calibration problem between PCUs. We selected only events detected in its top Xenon layer to maximise the signal to noise ratio(Jahoda et al. 2006). The background was modelled using the bright source model, that is appropriate for sources emitting > 40 c s^{-1} PCU^{-1}. We used the latest version (11.7) of the PCA response matrix generator, restricting to the 3–50 keV band and adding a systematic error of 0.5% to spectral counts[1]. Similarly to what was observed from other AMPs, the X-ray emission of IGR J17511–3057 is dominated by a power law–like emission extending to high (> 50 keV) energies. To model it we considered a simple thermal Comptonisation model (`nthcomp`, Zdziarski et al. 1996; Życki et al. 1999), fixing the

[1] N. Shaposhnikov, K. Jahoda, C. B. Markwardt, 2009, `http://www.universe.nasa.gov/xrays/programs/rxte/pca/doc/rmf/pcarmf-11.7/`

temperature of the hot electrons to 100 keV. Given the poor coverage of the PCA at low energies, we have also constrained the absorption column to nH = 1×10^{22} cm^{-2}, as it is suggested by an *XMM–Newton* observation performed during the same outburst (Papitto et al. 2010). A 6.6 keV emission line was also added to model residuals in the iron range, though such a feature is probably due to the contamination of the Galactic ridge in the field of view of the PCA (Markwardt et al. 2009b). The reduced chi square of the fit is good ($\chi^2_r = 64.3/72$). The unabsorbed flux we detect in the 3-50 keV band is $1.14(1) \times 10^{-9}$ erg cm^{-2} s^{-1}, that extrapolated in the 0.5-200 keV band gives an estimate of $\sim 2 \times 10^{-9}$ erg cm^{-2} s^{-1}. Under the hypothesis that emission is isotropic this corresponds to a bolometric luminosity of $L_x \sim 1.5 \times 10^{37}$ d$_8^2$ erg s^{-1}, where d$_8$ is the distance to the source in units of 8 kpc. We note here that an upper limit of 10.6 kpc on the source distance was set by Bozzo et al. (2009), by imposing that the burst peak luminosity does not exceed the Eddington limit, while Altamirano et al. (2010), from the analysis of the type-I bursts observed by *RXTE* and *Swift*, found an upper limit of 6.9 kpc. Papitto et al. (2010), on the basis of the spectral analysis of *XMM–Newton* data, gave also a lower limit of $\simeq$ 7 kpc, although derived under some assumptions. Moreover, as the source is only a few degrees away from the galactic centre and its X-ray emission is not heavily absorbed (nH $\sim 10^{22}$ cm^{-2}), it is highly probable that the distance does not exceed 8 kpc. Assuming that $L_X = \epsilon GM\dot{M}/R$ with $\epsilon \simeq 1$, we eventually deduce a peak mass accretion rate of the order of $\simeq 1.5 \times 10^{-9}$ d$_8^2$ M$_\odot$ yr^{-1}, which is the estimate we use in the following to compare the dynamical estimates of $\dot{M}$ from the timing analysis.

To describe the light curve shape, we chose to fit it with a piecewise linear function composed of three segments, as shown in Figure 1. We choose to fit only the first 23 days of data since the subsequent data are affected by the concomitant XTE J1751–305 outburst. We modelled each of the three intervals with a function $c_i(t) = c_i(1 - (t - T_i)/\tau_i), T_i \leq t < T_{i+1}$, where c_i is the count rate at $t = T_i$ and τ_i the linear decay timescale for the i-th piece. For the sake of simplicity we wrote this piecewise function as $c_0 f(t)$, where c_0 is the count rate at the peak. The best-fit result is reported in Figure 1.

2.2. Timing analysis

The spin frequency evolution in AMPs is thought to be driven by the accretion process. Matter falling from the accretion disk onto the NS transfers its angular momentum to the NS, which is spun-up to millisecond spin periods. But, as was evident from the first attempts (Ghosh et al. 1977), the magnetic field - accretion disk interaction can exert a negative torque onto the NS, spinning it down. This is called the threaded disk model. Due to the complexity of the problem, the details of the NS magnetosphere - disk interaction are still not well understood. In Literature three examples of AMPs which spin-down while accreting are reported (Galloway et al. 2002; Burderi et al. 2006; Papitto et al. 2008).

As already observed in other two AMPs (see e.g. Burderi et al. 2007 for SAX J1808.4–3658 and Riggio et al. 2008 for XTE J1807–294), also for this source the first harmonic is dominated by fluctuations and then unusable for our scope. It should be noted that the two AMPs cited above (SAX J1808.4–3658 and XTE J1807–294) show a second harmonic with a more regular behaviour.

An alternative interpretation of the pulse frequency derivatives was given by Hartman et al. (2008), who suggested that the red timing noise affecting the pulse phase delays can mimics a spin frequency derivative. Patruno et al. (2009) try to demonstrate that the pulse phase delays are correlated with the X-ray flux, rather than the genuine spin evolution of the source, due to motion of the hot-spot related to the flux. Unfortunately this correlation is not clear, even in the sign, in all AMPs and differs, in the same sources (see e.g. SAX J1808.4–3658 and XTE J1807–294), for each harmonic component, as noted by Patruno et al. (2009). We tested this hypothesis using the method as described in Patruno et al. (2009), adopting a constant spin frequency model to derive the pulse phase residuals. In the best-fit which maximise the linear correlation between phase residuals and flux we obtained $\chi^2_r \simeq 23$ (4625 / 201 d.o.f.), indicating that, for this source, the pulse phase residuals of the first harmonic cannot be ascribed to flux variation and/or fluctuations.

In the following, we will work under widely accepted hypothesis that the pulse frequency is the NS spin frequency. We will analyse the pulse phase delays and apply to them a disk threading model to derive the $\dot{M}$ and compare it with the value obtained from the spectral analysis of the same data.

We epoch folded data on time intervals of about 3.0 ks (one pulse profile per data file) and 32 phase bins. A third harmonic is detected during all the outburst. A fourth harmonic was also detected in the first 15 days of the outburst. In Figure 4, 5, 6 and 7 the first, second, third and fourth harmonic pulse phase delays are reported, respectively. The fractional amplitudes, as defined in Eq. 2, were corrected to take into account the instrumental background ($\sim$ 11 counts s^{-1} PCU^{-1} in the 2-25 keV energy band) and the background due to the presence of the galactic ridge in the field of view of *RXTE* (Markwardt et al. 2009b). To estimate this supplementary background we used the observations of the AMP XTE J1751–305 when both sources went to quiescence, in particular the observations from MJD 55115.400 to 55126.745, with a total exposure of 33.7 ks. Due to the low count rate, we used the faint background model, obtaining a count-rate of $\sim$ 7 counts s^{-1} PCU^{-1} in the same energy band. In Figure 8 the fractional amplitudes for the four harmonics are reported.

The mean spin frequency reported in Table 1 is obtained by fitting the first harmonics pulse phase delays with a constant spin frequency model. The value obtained in this way for the spin frequency is $\nu = 244.8339515569(24)$ Hz. However, the systematic effects due to the uncertainty of 0.6″ (Nowak et al. 2009) on the source position brings the mean spin frequency error to 7×10^{-8} Hz (see Burderi et al. 2007).

2.2.1. First harmonic

We started fitting the first harmonic pulse phase delays with a constant spin frequency derivative in order to have an estimate of the mean spin frequency derivative. From the fit we obtained $\dot{\nu} = -7.0(9) \times 10^{-14}$ Hz s^{-1} with a $\chi^2_r = 18.51(3869/209)$, clearly unacceptable.

In order to improve this result we used the threaded disk model applied to the AMPs by Rappaport et al. (2004). According to this model, the net torque acting on an AMP is:

$$\tau(t) = 2\pi I \dot{\nu}(t) = \dot{M}(t)\sqrt{GMR_c} - \frac{\mu^2}{9R_c^3}, \qquad (4)$$

where I is NS moment of inertia, $\dot{M}$ is the mass accretion rate, M is the mass of the NS, μ is the magnetic dipole moment of the NS and R_c the co-rotation radius.

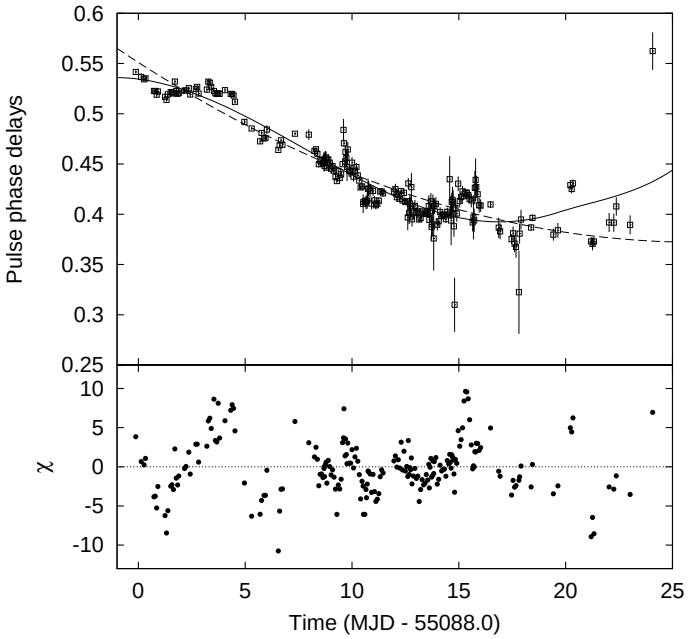

Figure 4. In the top panel we show the first harmonic pulse phase delays and the best-fitting curves, considering a constant spin frequency derivative (dashed line) and the disk threading model proposed by Rappaport et al. (2004). In the bottom panel we show the residuals (in σ units) of the first harmonic with respect to the best fitting model given by the threaded disk.

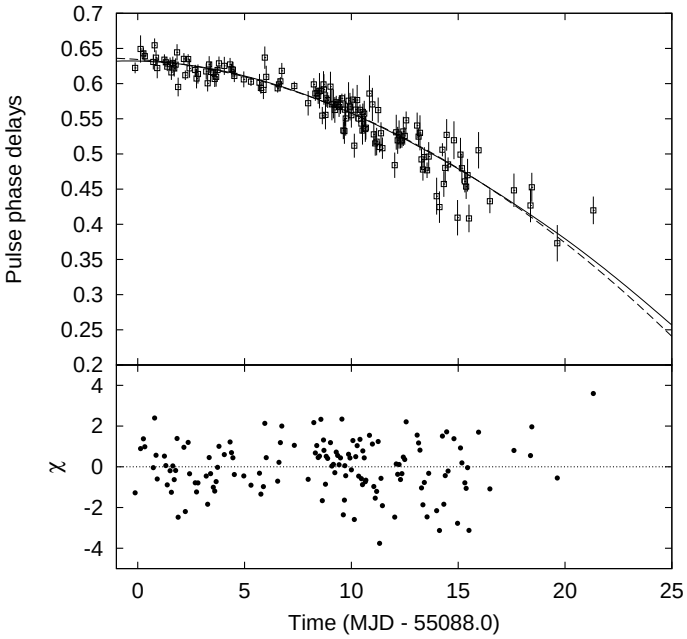

Figure 5. In the top panel of this figure the second harmonic pulse phase delays are shown. The dashed and the continuous lines are the second harmonic best-fit curves considering a constant spin frequency derivative and the physical model considering the material torque proportional to the flux, respectively. In the bottom panel the residuals (in σ units) of the second harmonic with respect the constant spin frequency derivative are shown.

To apply this model to our data we need an expression for $\dot{M}(t)$. We then made the hypothesis that the bolometric luminosity L(t) is a good tracer of $\dot{M}$. In the hypothesis that the spectral variation during the outburst is not significant it is possible to consider L(t) proportional to the background subtracted count rate. We can then write $\dot{M}(t) = \dot{M}_{max} f(t)$, where $\dot{M}_{max}$ is the maximum accretion rate in correspondence of the flux peak and f(t) is the functional form of the count rate previously derived.

An expression for $\dot{\nu}$ as function of $\dot{M}$ can easily be derived from Eq. 4:

$$\dot{\nu}(t) = \left[1.427\ \frac{m^{2/3} P_{-3}^{1/3} \dot{M}_{-10}^{max}}{I_{45}} f(t) - 5.232\ \frac{\mu_{26}^2}{m I_{45} P_{-3}^2}\right] \times 10^{-14}\ \mathrm{Hz\ s^{-1}}, \quad (5)$$

where m is the NS mass in units of $M_\odot$, $\dot{M}_{-10}^{max}$ is the maximum mass accretion rate in units of 10^{-10} $M_\odot$ y^{-1}, P_{-3} the spin period in units of 10^{-3} s and I_{45} the NS moment of inertia in 10^{45} gr cm^2. In this work we adopted the FPS (Friedman Pandharipande Skyrme, see Friedman & Pandharipande 1981; Pandharipande & Ravenhall 1989) equation of state for which, fixing NS mass to $M = 1.4 M_\odot$, we obtain a radius of $R_{NS} = 1.14 \times 10^6$ cm and a moment of inertia $I = 1.29 \times 10^{45}$ gr cm^2.

The pulse phase delays formula used for the fit is obtained doubly integrating the expression 5 with respect to the time (see e.g. Burderi et al. 2007).

From the fit of the first harmonic we obtained a magnetic dipole strength of $\mu = 1.64(7) \times 10^{27}$ G cm^3 and $\dot{M}_{max} = 5.7(6) \times 10^{-9}$ $M_\odot$ y^{-1}, with a $\chi_r^2 = 12.36(2570/208)$, still unacceptable. The results are reported in Figure 4. Such a big χ_r^2 is clearly due to fluctuations in the pulse phase delays, as it is possible to see in the best-fit residuals reported in Figure 4 (bottom panel). As foretold, we unsuccessfully try to interpret it with the model suggested by Patruno et al. (2009). The origin of such fluctuations still remains unexplained.

2.2.2. Second harmonic

Considering the second harmonic less affected by phase noise (Burderi et al. 2006; Riggio et al. 2008), we repeated the fitting procedure using these phase delays. In the constant spin frequency derivative case we obtained $\dot{\nu} = 1.45(16) \times 10^{-13}$ Hz s^{-1} with a $\chi_r^2 = 1.74(238.5/137)$. The best-fit curve is reported in Figure 5. We adopted the same disk threading expression used for the first harmonic to describe the second harmonic. In this case we had to fix $\mu = 0$ since μ and $\dot{M}_{max}$ strongly correlate. In this case, therefore, the derived value of $\dot{M}_{max}$ has to be considered as a lower limit to the mass accretion rate at the peak of the outburst, since value of the magnetic moment higher than zero will give a higher value for $\dot{M}_{max}$. The best-fit results are reported in Table 1. In this case the best-fit value of $\dot{M}_{max} = 0.92(10) \times 10^{-9}$ $M_\odot$ year^{-1}, with a $\chi_r^2 = 1.70(232.8/137)$, is in good agreement with our estimate from the bolometric flux for a source distance of about 6.3(3) kpc.

2.2.3. Third harmonic

Since in this source the third harmonic is significantly detected in nearly the whole outburst we proceeded with the same method used for the first and second harmonic. From the fit with the constant spin frequency derivative we obtained $\nu = 244.83395151(6)$ Hz and $\dot{\nu} = 4.8(1.4) \times 10^{-14}$ Hz s^{-1} with a $\chi_r^2 = 1.58(159.8/101)$. The best-fit curve is reported in Figure 6. We applied the threaded disk model to describe the third harmonic and, as already done for the second harmonic, we fixed $\mu = 0$ since μ and $\dot{M}_{max}$ correlate in the fit. The obtained best-fit values are $\dot{M}_{max} = 3.1(9) \times 10^{-10}$ $M_\odot$ year^{-1} for the peak mass accretion rate and $\nu = 244.83395150(6)$ Hz with a reduced χ^2 of $\chi_r^2 = 1.57(159.0/101)$. The third harmonic shows a spin-up, although not highly significant ($\gtrsim 3\sigma$ c.l.). The peak mass accre-

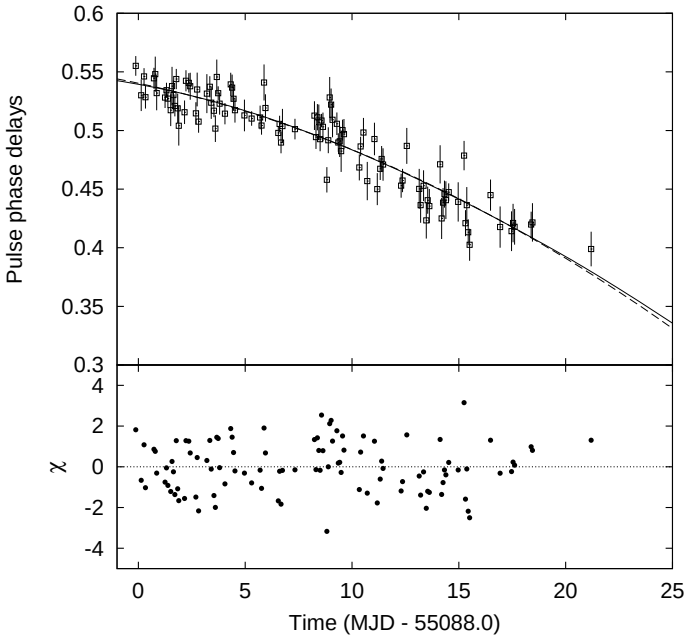

Figure 6. In the top panel of this figure the third harmonic pulse phase delays and its best-fit curves considering a constant spin frequency derivative (dashed line) and the physical model considering the material torque proportional to the flux (continuous line) are reported. In the bottom panel we show the residuals in units of σ with respect the constant spin frequency derivative model.

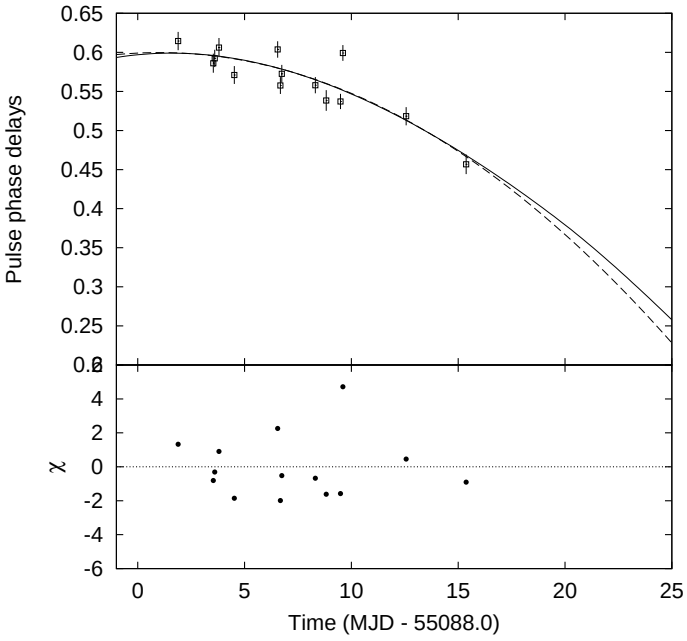

Figure 7. In the top panel of this figure the fourth harmonic pulse phase delays and its best-fit curves considering a constant spin frequency derivative (dashed line) and the physical model considering the material torque proportional to the flux (continuous line) are reported. In the bottom panel we show the residuals in units of σ with respect the constant spin frequency derivative model.

tion rate deduced is quite low in comparison to the one obtained from the bolometric flux for a source distance of 6.3(3) kpc. In fact the source distance is of 3.6(5) kpc.

2.2.4. Fourth harmonic

The fourth harmonic is sporadically detected in the first 15 days of the outburst, with a fractional amplitude of $\sim 1\%$. From the fit with the constant spin frequency derivative we obtained $|\dot{\nu}| < 2.7) \times 10^{-13}$ Hz s^{-1} (2σ c.l.) with a $\chi^2_r = 4.03(44.28/11)$. The best-fit curve is reported in Figure 7. The obtained best-fit values are $\dot{M}_{max} < 1.6 \times 10^{-9}$ M$_\odot$ year^{-1} (2σ c.l.) for the peak mass accretion rate with a reduced χ^2 of $\chi^2_r = 4.09(45/11)$.

It should be noted that, as already done in Burderi et al. (2007) and Riggio et al. (2008), we taken into account the effect of the source position uncertainty on the obtained values of ν and $\dot{\nu}$, adopting the same method described in Riggio et al. (2008). In particular, in the case of constant spin frequency derivative the uncertainties are of $\Delta\nu = 6.1 \times 10^{-8}$ Hz on the frequency and $\Delta\dot{\nu} = 0.72 \times 10^{-14}$ Hz s^{-1} on the spin frequency derivative, while in the case of the physical model the uncertainties are of $\Delta\nu = 6.1 \times 10^{-8}$ Hz on the frequency and $\Delta\dot{M} = 4.3 \times 10^{-11}$ M$_\odot$ y^{-1} on the peak accretion rate.

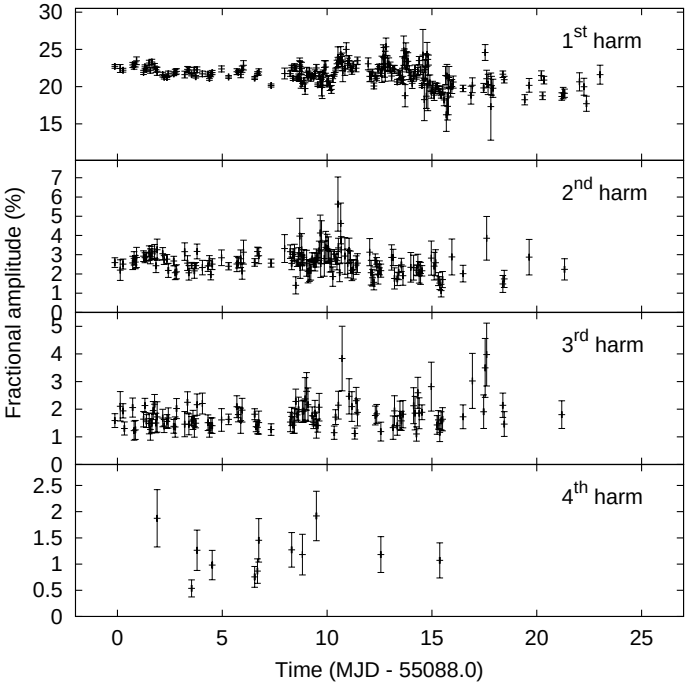

Figure 8. The fractional amplitudes of the four harmonics are reported. Points in correspondence of the type-I bursts are not plotted due to difficult estimate of the persistent flux.

2.3. Spectral variability of the pulse profile

As already done by Papitto et al. (2010) analysing the *XMM–Newton* observation of the same outburst, we analysed the energy dependence of phase and amplitude of the three harmonic components. In order to have a good statistics we epoch folded data from 55089.233 MJD to 55092.5379 MJD, excluding the three data files where a type-I burst was present, with an exposure of 81 ks and a coverage of 28%. We choose this interval because the pulse phase delays have a quite stable linear trend with an average first harmonic phase scattering of 0.005. We consider only data from PCU2. We evaluated also the contribution to the background given by the galactic bulge, using the data described in the previous section, in the working hypothesis that the changes due to the different observation data and slightly different instrument pointing are small (see Papitto et al. 2010,

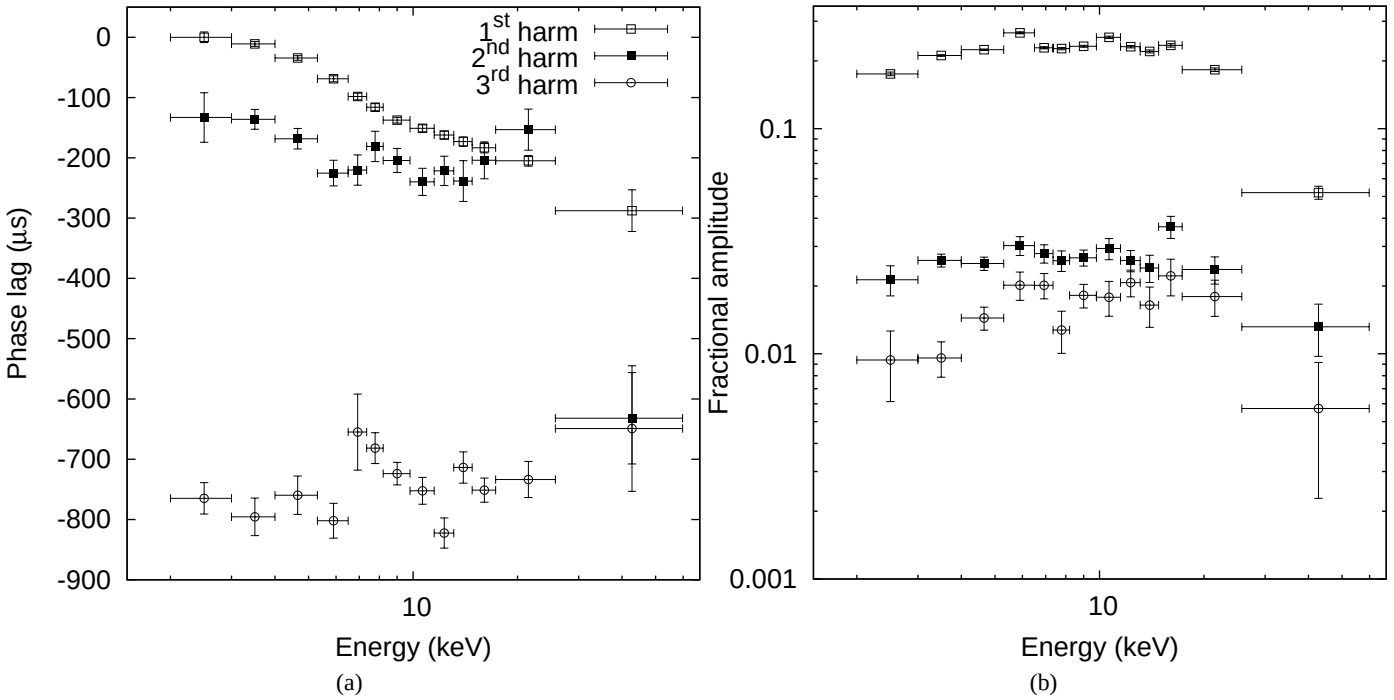

Figure 9. In the left panel the phase lags for the first three harmonics are reported. The phase lags are measured with respect to the maxima of each component, as done in Papitto et al. (2010). In the right panel the fractional amplitude for the three harmonics are reported.

for a detailed discussion). For these reasons small systematics could be present and the confidence intervals could be underestimated. The fractional amplitude of the first harmonic (Fig. 9, right panel) increases from 17.5(3)% at 2.5 keV to 26.7(3)% at 6 keV. It remains roughly constant around 23% up to 12 keV, where the fractional amplitude is 25.4(3)%. Above 12 keV there is a steady decline of the fractional amplitude, although up to the energy band 25-60 keV is still well detectable with a fractional amplitude of 5.2(3)%. The second and third harmonic fractional amplitudes show a behaviour similar to the first harmonic one, increasing with energy with a maximum (around 10-20 keV) of 3.7(4)% and 2.2(4)%, respectively. We also observe a decline of the fractional amplitude above 20 keV for these harmonics. Fractional amplitudes as a function of photon energies were not clearly detected for the fourth harmonic, probably due to the long time of integration and the smearing caused by the observed fourth harmonic phase fluctuations of ~ 0.05 (see Fig. 7), which is a considerable fraction of the fourth harmonic period.

The first harmonic show phase lags (reported in Fig. 9, left panel). As described in Papitto et al. (2010), there is a steady decrease of the phase lag up to $\sim$ 10 keV, where it is clearly visible a break. Beyond 10 keV the pulse phase lag still decrease, but with a smaller rate.

The second harmonic shows a different trend with respect to the first harmonic. It reaches the maximum lag around 10 keV, it shows no time lag at 25 keV, but then we observe a sudden jump of $\sim -450\mu$s from 25 to 50 keV.

The third harmonic phase lags are roughly constant in all the energy band. It should be noted that in the energy band 25.7–59.8 keV the phase lags for the second and the third coincide.

2.4. type-I bursts timing

We performed a timing analysis of all the 10 type-I burst present in the observation, with the goal of studying the pulse profile evolution during the burst. In Figure 10 we show the results for the second and fifth type-I burst, the best sampled among the bursts present in the *RXTE* observation. The starting date of these bursts is 55089.721 MJD (TDB) and 55094.619 MJD (TDB), and the decay time is 8.0(1) seconds and 8.5(1) seconds, respectively. We divided each burst in chunks holding (roughly) the same number of events so that in each folded profile a fractional amplitude of $\sim$ 20% can be easily detectable. We folded each chunk using 8 phase bins and performed an harmonic decomposition using only the first harmonic. The results of this analysis are reported in Figure 10. During both bursts, the pulse phase delays remain stable and, with the exception of the very first seconds, locked to the pulse phase delays during the persistent emission (see Figure 10, mid panel). The fractional amplitude behaviour is even more interesting because remains, within the errors, quite constant during both bursts and locked to the persistent value (Figure 10, bottom panel). A detailed spectral and temporal analysis of all these type-I bursts was recently reported by Altamirano et al. (2010), although with different techniques.

3. Discussion

Among the AMPs known, IGR J17511–3057 shows several peculiarities. The source shows the highest persistent first harmonic fractional amplitude with a peak value (background corrected) at the beginning of the outburst of about 23% which linearly decrease to 17% at the end of the outburst (see Figure 8), while the highest ever observed fractional amplitude was observed by Patruno et al. (2010) in XTE J1807–294.

The pulse shape is complex, showing, on integration times of 3 ks, a second harmonic, a third harmonic and sporadically a fourth harmonic with fractional amplitudes of 2.5%, 1.6% and 1%, respectively (see Figure 8). A third harmonic as strong as the second harmonic could be, following Poutanen & Beloborodov (2006), an indication that both hot spots are visible with the sec-

ondary spot only partially visible, since for a single spot the third harmonic should be much smaller than the second harmonic ($a_2/a_3 \gtrsim 5$, Poutanen & Beloborodov 2006), suggesting intermediate values for the inclination angle. In the AMPs, Hartman et al. (2008) reports of a sporadically detectable third harmonic in SAX J1808.4–3658, while Patruno et al. (2010) detected sporadically a third and a fourth harmonic in XTE J1807–294.

The fact that in IGR J17511–3057 the third harmonic is visible for nearly all the outburst with a total of 105 detections over 216 folded pulse profiles makes this source peculiar.

Moreover, while the fractional amplitude of the first harmonic clearly shows a steady decrease with the flux, such a decrease is less evident in the second and third harmonics, for which the fractional amplitude remains more stable when the X-ray flux decreases (see Figure 8).

However, the most interesting and puzzling result is the different behaviour of the phase delays of the four harmonic components. In particular, similarly to other AMPs, such as SAX J1808.4–3658 and XTE J1807–294 (see e.g. Burderi et al. 2007; Hartman et al. 2008, 2009; Riggio et al. 2008; Patruno et al. 2010), the first harmonic shows clear phase fluctuations (see Figure 4). A discussion over the results based on the analysis of the first harmonic is strongly affected by these phase fluctuations. We can only do some hypotheses on the nature of such fluctuations. The amplitude of these fluctuations, ~ 0.05 in phase units, could corresponds to hot spot movements of ~ 18 degrees, already seen in numerical simulations (see Romanova et al. 2004; Bachetti et al. 2010), although on time-scales of fraction of seconds, while the observed time-scales are of few days. We also tried to interpret these phase fluctuations with the model suggested by Patruno et al. (2010). We adopted a constant spin frequency model and a linear relation between flux and pulse phase residuals. The best correlation parameter set gave a $\chi^2_r \simeq 23$, clearly unacceptable. A model to describe and correctly interpret these fluctuations is still missing.

However, under the working hypothesis that some exchange of angular momentum between the NS and the accreting matter has to occur during X-ray outbursts, when the accretion rate is at its maximum, we try to interpret the behaviour of the phase delays of the second and third harmonic, which appear to be less affected by phase fluctuations. The fact that the phase delays derived from the second harmonic appear more stable than those derived from the first harmonic has been observed, for instance, during the 2002 outburst from SAX J1808.4–3658. Burderi et al. (2007) showed that, while the first harmonic phase delays clearly show a phase shift at days 14 from the beginning of the 2002 outburst, a similar phase shift was not present in the phase delays derived from the second harmonic. A similar behaviour was also observed by Riggio et al. (2008) for the AMP XTE J1807–294, which went onto outburst just once in 2003 in the *RXTE* era. In both these cases, the interpretation of the phase delays derived from the second harmonic in terms of accretion torques provided reasonable spin frequency derivatives (and inferred mass accretion rates onto the NS), although a different interpretation was given for both sources by Hartman et al. (2009); Patruno et al. (2009). Naturally, these results have to be taken with great caution, since it is not excluded that phase fluctuations can still affect phase delays derived from the second (or higher) harmonic.

In the case of IGR J17511–3057, again, the second harmonic shows a more regular behaviour with respect to the first harmonic and suggests a spin-up of the NS (see Figure 5). From the fit with our simplified torque model we obtain an $\dot{M}$ estimate, fixing $\mu = 0$, of $\dot{M}_{\rm max} = 0.92(10) \times 10^{-9}$ M$_\odot$ year^{-1}, which would be compatible with the observed X-ray flux from the source if we put the source at a distance of 6.3 kpc. This could indirectly suggest that the second harmonic component is a better tracer of the spin frequency evolution, even if a physical model that explains all the phenomenology observed in all the AMPs class is still missing. Results obtained on the second harmonic give, as in the case of the AMPs SAX J1808.4–3658 (Burderi et al. 2006; Hartman et al. 2009) and XTE J1807–294 (Riggio et al. 2008), reasonable values for the physical parameters of the system.

However, if we look at the third harmonic we find that it shows a spin-up although it is not highly significant ($\gtrsim \mathbf{3}\sigma$) and smaller than the value inferred from the second harmonic. The lower limit to the accretion rate $\dot{M}_{\rm max} = 3.1(9) \times 10^{-10}$ M$_\odot$ year^{-1} gives a distance of 3.6(5) kpc, at $\sim 5\sigma$ from the value inferred from the second harmonic. This value is not compatible with the second harmonic one. The lack of literature and observations of the third harmonic behaviour in other AMPs does not allow to make a comparison with other cases, leaving the question open.

A fourth harmonic was sporadically detected during the outburst. We tried to fit the pulse phase delays with the same models adopted for the other harmonics but the result is inconclusive. It should be noted that is affected by a phase fluctuations (~ 0.02) comparable with the first harmonic's fluctuations. It is probable that integrating on long time-scales, the large fluctuations make its detection unfeasible.

We performed a high resolution timing analysis of all the type-I bursts present in this *RXTE* observation. The results are very similar for all the bursts, and we show the burst 2 and 5 (see Figure 10) since these are the best sampled in the *RXTE* observation. The first harmonic phase delays appear to rise in correspondence of the fast rising phase of the burst, suggesting a frequency drift during the first few seconds since the burst onset (Altamirano et al. 2010), and to return to the phase value during the persistent emission during the burst decay, giving some evidence that the burst probably starts not far from the hot spot in the polar cap. The fractional amplitude in each burst remains instead locked (within the errors) to the persistent emission value during all the burst, suggesting the quite surprising fact that the temperature gradient does not vary during the burst. An interpretation of a such behaviour is beyond the scope of this work.

From the orbital ephemeris reported in Table 1 the pulsar mass function is $f_X = 1.070854(21) \times 10^{-3}$ M$_\odot$. From this value of mass function we can derive a minimum mass for the companion star of 0.14 M$_\odot$, considering an inclination angle of 90^o and a NS mass of 1.4 M$_\odot$. With such a minimum mass, the companion star of IGR J17511–3057 is one of the more massive companion stars among the AMPs, together with XTE J1807–294 and SAX J1748.9–2021 (Altamirano et al. 2008). Using the relation $R_{RL_2} = 1.2 \times 10^{10} m_{2,0.1}^{1/3} P_{2h}^{2/3}$ cm (Paczyński 1971), where $m_{2,0.1}$ is the companion mass in 0.1M$_\odot$ units and P_{2h} is the orbital period in two hours units, we obtain for the companion's Roche lobe radius a value of 0.248 R$_\odot$. Such value is larger than what is expected for a low mass main sequence star (see Chabrier & Baraffe 2000, 5 Gyr track), for which the corresponding radius is about 0.15 R$_\odot$. It can be shown that the contact condition between Roche lobe and companion star pose a firm lower limit to the inclination of the system of ~ 20 degrees, corresponding to a companion mass of ~ 0.45M$_\odot$. For smaller inclination angles the companion star would overfill its Roche lobe. This obviously excludes that the companion star could be a white dwarf or an helium-core star, while strongly suggests that the companion star is a main sequence star, possibly bloated as a consequence of its evolutionary history (Podsiadlowski et al. 2002). The nature

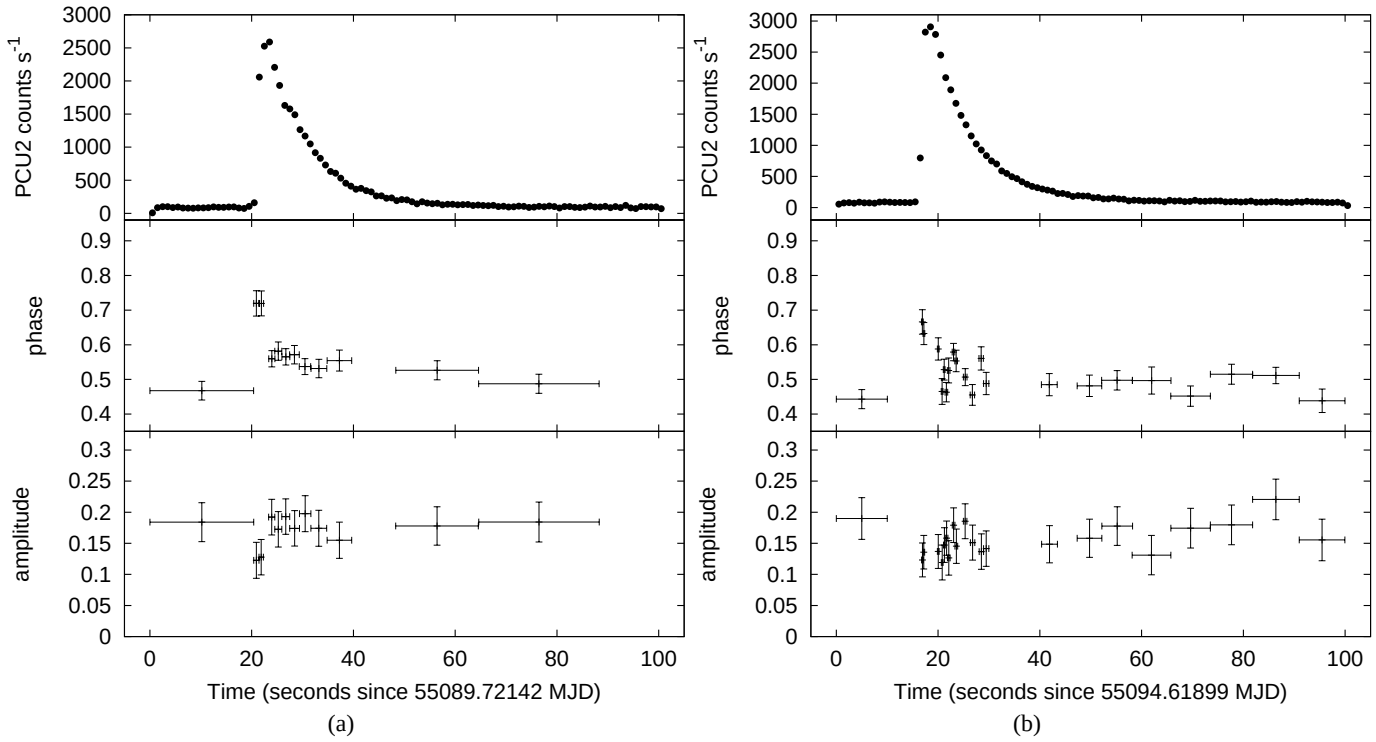

Figure 10. Two type-I burst timing analysis is reported. For each burst in the top panel the PCU2 count rate of the type-I burst present in this observation, in the mid panel the pulse phase delays and in the bottom panel the fractional amplitude are reported.

of the companion star is thoroughly discussed in Papitto et al. (2010).

Acknowledgements. We thank the anonymous referee for having help us to greatly improve the paper.
We also thank Sergey B. Popov for several fruitful discussions.
This work is supported by the Italian Space Agency, ASI-INAF I/088/06/0 contract for High Energy Astrophysics.

References

Altamirano, D., Casella, P., Patruno, A., Wijnands, R., & van der Klis, M. 2008, ApJ, 674, L45
Altamirano, D., Watts, A., Linares, M., et al. 2010, ArXiv e-prints
Bachetti, M., Romanova, M. M., Kulkarni, A., Burderi, L., & di Salvo, T. 2010, MNRAS, 146
Baldovin, C. 2009, The Astronomer's Telegram, 2196, 1
Bevington, P. R. & Robinson, D. K. 2003, Data reduction and error analysis for the physical sciences, 3rd edn. (McGraw-Hill)
Bozzo, E., Ferrigno, C., Falanga, M., et al. 2009, ArXiv e-prints
Burderi, L., Di Salvo, T., Lavagetto, G., et al. 2007, ApJ, 657, 961
Burderi, L., Di Salvo, T., Menna, M. T., Riggio, A., & Papitto, A. 2006, ApJ, 653, L133
Chabrier, G. & Baraffe, I. 2000, ARA&A, 38, 337
Chenevez, J., Kuulkers, E., Beckmann, V., et al. 2009, The Astronomer's Telegram, 2235, 1
Deeter, J. E., Pravdo, S. H., & Boynton, P. E. 1981, ApJ, 247, 1003
Friedman, B. & Pandharipande, V. R. 1981, Nuclear Physics A, 361, 502
Galloway, D. K., Chakrabarty, D., Morgan, E. H., & Remillard, R. A. 2002, ApJ, 576, L137
Ghosh, P., Pethick, C. J., & Lamb, F. K. 1977, ApJ, 217, 578
Hartman, J. M., Patruno, A., Chakrabarty, D., et al. 2008, ApJ, 675, 1468
Hartman, J. M., Patruno, A., Chakrabarty, D., et al. 2009, ApJ, 702, 1673
Jahoda, K., Markwardt, C. B., Radeva, Y., et al. 2006, ApJS, 163, 401
Leahy, D. A., Elsner, R. F., & Weisskopf, M. C. 1983, ApJ, 272, 256
Markwardt, C. B., Altamirano, D., Strohmayer, T. E., & Swank, J. H. 2009a, The Astronomer's Telegram, 2237, 1
Markwardt, C. B., Altamirano, D., Swank, J. H., et al. 2009b, The Astronomer's Telegram, 2197, 1
Miller-Jones, J. C. A., Russell, D. M., & Migliari, S. 2009, The Astronomer's Telegram, 2232, 1
Nowak, M. A., Paizis, A., Wilms, J., et al. 2009, The Astronomer's Telegram, 2215, 1
Paczyński, B. 1971, ARA&A, 9, 183
Pandharipande, V. R. & Ravenhall, D. G. 1989, in NATO ASIB Proc. 205: Nuclear Matter and Heavy Ion Collisions, ed. M. Soyeur, H. Flocard, B. Tamain, & M. Porneuf, 103–+
Papitto, A., Menna, M. T., Burderi, L., di Salvo, T., & Riggio, A. 2008, MNRAS, 383, 411
Papitto, A., Riggio, A., Burderi, L., et al. 2009, The Astronomer's Telegram, 2220, 1
Papitto, A., Riggio, A., Di Salvo, T., et al. 2010, ArXiv e-prints
Patruno, A., Hartman, J. M., Wijnands, R., Chakrabarty, D., & van der Klis, M. 2010, ApJ, 717, 1253
Patruno, A., Wijnands, R., & van der Klis, M. 2009, ApJ, 698, L60
Podsiadlowski, P., Rappaport, S., & Pfahl, E. D. 2002, ApJ, 565, 1107
Poutanen, J. & Beloborodov, A. M. 2006, MNRAS, 373, 836
Rappaport, S. A., Fregeau, J. M., & Spruit, H. 2004, ApJ, 606, 436
Riggio, A., di Salvo, T., Burderi, L., et al. 2007, MNRAS, 382, 1751
Riggio, A., Di Salvo, T., Burderi, L., et al. 2008, ApJ, 678, 1273
Riggio, A., Papitto, A., Burderi, L., et al. 2009, The Astronomer's Telegram, 2221, 1
Romanova, M. M., Ustyugova, G. V., Koldoba, A. V., & Lovelace, R. V. E. 2004, ApJ, 610, 920
Torres, M. A. P., Jonker, P. G., Steeghs, D., Simon, J. D., & Gutowski, G. 2009, The Astronomer's Telegram, 2216, 1
van den Heuvel, E. P. J. 1984, Journal of Astrophysics and Astronomy, 5, 209
Zdziarski, A. A., Johnson, W. N., & Magdziarz, P. 1996, MNRAS, 283, 193
Życki, P. T., Done, C., & Smith, D. A. 1999, MNRAS, 309, 561